

NAT'L INST. OF STAND & TECH  
A11106 038726

REFERENCE

NIST  
PUBLICATIONS

NBSIR 82-2574

# Analysis of Oxide and Oxide/Matrix Interfaces in Silicon Nitride

---

U.S. DEPARTMENT OF COMMERCE  
National Bureau of Standards  
National Measurement Laboratory  
Center for Materials Science  
Fracture and Deformation Division  
Washington, DC 20234

July 1982

Interim Report

NBS-DOE Interagency Agreement EA-77-A-01-6010

Prepared for  
Department of Energy  
Fossil Fuel Utilization Division  
Washington, DC

QC  
100  
.U56  
82-2574  
1982



NBSIR 82-2574

## **ANALYSIS OF OXIDE AND OXIDE/MATRIX INTERFACES IN SILICON NITRIDE**

---

U.S. DEPARTMENT OF COMMERCE  
National Bureau of Standards  
National Measurement Laboratory  
Center for Materials Science  
Fracture and Deformation Division  
Washington, DC 20234

July 1982

Interim Report

NBS-DOE Interagency Agreement EA-77-A-01-6010

Prepared for  
Department of Energy  
Fossil Fuel Utilization Division  
Washington, DC



---

U.S. DEPARTMENT OF COMMERCE, Malcolm Baldrige, *Secretary*  
NATIONAL BUREAU OF STANDARDS, Ernest Ambler, *Director*



# ANALYSIS OF OXIDE AND OXIDE + MATRIX INTERFACES IN SILICON NITRIDE

Nancy J. Tighe

National Bureau of Standards

Washington, DC 20234

## ABSTRACT

In order to understand the strength and microstructural changes that are produced during oxidation, it is necessary to examine the oxide scale, the oxide:silicon nitride interface and the silicon nitride below the oxide:matrix interface. In the present study, these three interfacial layers were removed and analyzed using transmission electron microscopy, light microscopy, x-ray energy analysis and x-ray diffraction. Oxide scales were produced on hot-pressed silicon nitride samples by heating in air at 1000 °C, 1200 °C, and 1400 °C for 1/2 to 1000 hr. The phases in the oxide scale were found to occur in layers that were ordered according to the phase diagrams for the oxide mixtures. Crystalline and amorphous phases were present in all specimens examined. The oxynitride and amorphous phases are present in as-pressed billets at triple junctions and along grain boundaries. The elements in the amorphous phases were identified using energy dispersive x-ray analysis. In this paper, the phases found in the oxide scales are characterized and the relationships between the oxide scale, the oxide:matrix interface and the mechanical properties are discussed.

## I. INTRODUCTION

Oxide phases occur in hot-pressed silicon nitride billets as a result of processing and in silicon nitride components as a result of exposure to air at elevated temperatures. During processing, the oxides act as sintering aids and form as thin (approx. 1nm) films around grains [1,2]; as massive second phases at triple junctions; and, as fillers of void space [3]. The internal oxides and the oxide scale formed during heating in air at elevated temperatures consist of several discrete phases which can be either amorphous or crystalline [3,4]. The oxide phases modify the silicon nitride microstructure and can have the effect of strengthening or of weakening a particular component depending on the formation parameters.

Silicon nitride is a brittle ceramic which fails under stress by crack propagation from a flaw which has reached a critical size as defined by the stress intensity factor  $K_c$  [5]. At sufficiently high temperature the material can creep under an applied stress and can fail by crack propagation and plastic deformation. Cavitation and separation of grains along their boundaries eventually leads to creep rupture [6,7]. The flaw population in machined silicon nitride specimens includes cracks produced during surface finishing; and, internal inclusions and pores which were produced during processing of the original billet. Extensive measurements of strength and analyses of the durability and reliability of hot-pressed silicon nitride billets have demonstrated conclusively that the flaw population changes continuously during heating in air [6,8,9]. The changes in flaw population are divided into two categories (a) flaw healing, whereby the size and effectiveness of initial flaws are reduced; and, (b) flaw generation, whereby

new flaws such as surface pits, grain boundary cracks and internal oxide inclusions are produced. The effects of the new flaw population on strength distribution are less predictable than effects of initial machining flaws because they are produced in a time and stress dependent manner and are changing continuously. New techniques have been developed to predict the reliability of the materials [10] but will not be discussed in this paper. The techniques used to identify flaw populations and their influence on the material strength will be discussed.

In order to identify the microstructural changes that occurred during heating in air we examined the oxide scale, the oxide : silicon nitride interface and the silicon nitride beneath the oxide : matrix interface. Samples were oxidized by heating in air at 1000°C, 1200°C and 1400°C for 1/2 to 1000 hours. The interfacial layers were removed and examined by transmission electron microscopy, light microscopy, energy dispersive x-ray spectroscopy, and in x-ray diffraction procedures. The strength changes that were measured for silicon nitride after heating in air to cause oxidation resulted from changes in microstructure near the oxide : matrix interface. Because of the overwhelming evidence for diffusion from the matrix to the outer oxide interfaces in this paper and in earlier papers [3] we have termed this interface area the diffusion reaction zone.

## II. EXPERIMENTAL PROCEDURE

Specimens examined during this study were made from billets of hot-pressed magnesia-doped  $\text{Si}_3\text{N}_4$  designated HS130 and NC132. Specimens thin

enough for examination in a transmission electron microscope were made from oxidized specimens by sectioning them parallel to the oxide/silicon nitride interface; grinding the section to include the desired portion of the oxide layer, polishing the thin section to show the oxide phases, and then ion-thinning until the desired area was electron transparent.

The oxidation treatments were carried out on thin foil specimens as well as on bulk samples. Small specimens were held vertically in a silicon nitride boat and larger bars or plates were supported at the ends on silicon nitride or silicon carbide plattens. Thus, there was no direct contact with an oxide ceramic or a metal foil which would cause an undesirable chemical reaction. Specimens were weighed and measured before and after oxidation in order to record the oxide scale growth. The oxide scale on some specimens was dissolved in  $\text{HF}+\text{H}_2\text{SO}_4$  in order to establish the depth of oxide penetration into the matrix. Specimens from mechanical tests had been heated in air at  $1000^\circ\text{C}$ ,  $1200^\circ\text{C}$ , and  $1400^\circ\text{C}$  for times of 1/2 to 1000 hr.

### III. EXPERIMENTAL RESULTS

#### (1) OXIDE PHASES

When the surface and cross-sections of heavily oxidized specimens were examined it was found that the oxide scale had formed in layers that differed in composition ( $\text{Si}_2\text{N}_2\text{O}+\text{SiO}_2$  and  $\text{SiO}_2+\text{MgSiO}_3$ ) and in crystallinity. As shown in Fig. 1, certain oxide phases could be distinguished easily by light microscopy because of large differences in the index of refraction and the reflectivity. In samples that were machined to have sharp edges, corner or

edge cracks were extended during bending. The crack interfaces oxidized preferentially and were seen easily in polished sections. A plate 1 mm thick which was oxidized at 1400 °C for 112 hours sagged as a result of the exposure indicating that creep and plastic deformation had taken place. Thickness measurements of the oxide scale, which were made from cross-sections of hot-pressed (NC 130) samples heated at 1400 °C, are shown in Fig. 1(c). It is seen that the scale thickness did not change appreciably from 4-24 hours exposure; but, did increase for the 48 and 112 hour exposures. This is consistent with the appearance of magnesium silicate phases in these specimens as determined from X-ray powder diffraction patterns. The oxide scale on a plate that was heated cyclically at 1400 °C for 96 hours showed globules of silicate which were considered evidence for melting (Fig. 1b). Such melting can be attributed to the gradual change in composition of the oxide surface which enhanced the oxidation rate compared with continuously heated samples.

Silicon Oxynitride :  $\text{Si}_2\text{N}_2\text{O}$  [11,12] Silicon oxynitride was found in the hot-pressed billets in sufficient quantity to be identified in x-ray powder diffraction patterns. When polished sections were examined in the light microscope, the oxynitride could be distinguished from the silicon nitride matrix by its darker grey color which results from the difference in reflectivity ( $r$ ), and index of refraction ( $n$ ):  $\text{Si}_3\text{N}_4$   $r=12.2$ ,  $n=2.1$ ;  $\text{Si}_2\text{N}_2\text{O}$   $r=8.5$ ,  $n=1.82$  [13]. In the light micrograph of Fig. 1d, spherical oxide nodules are visible below the matrix/oxide interface. The smallest nodules are oxynitride. In the center of the larger nodules the silicate phase is visible; thus, indicating a more complete oxidation reaction. The position of the nodules below the reaction interface is strong evidence for significant diffusion of oxygen into the matrix at 1400 °C.

The electron micrographs in Fig. 2a,b show the structure of the oxynitride phase in a thin foil specimen prepared from a section similar to m-m in Fig. 1c. The lower magnification picture of Fig. 2a shows two oxynitride grains with a region of silicon nitride grains between them. In Fig. 2b the faults, pores and inclusions within one of the oxynitride grains are imaged. It is apparent that the initial silicon nitride grains were consumed by the growing oxynitride.

Cristobalite- $\beta\text{SiO}_2$ . Beta-cristobalite was found along the silicon nitride interfaces in specimens oxidized at 1000 °C and throughout the oxide scale in specimens oxidized at 1400 °C. The cristobalite was found in quenched samples as well as in heated samples that were oxidized at 1000 °C and 1200 °C in a special high temperature x-ray furnace. The phase coexisted with an amorphous phase which appeared to be silica from its diffraction pattern.

Figure 3 shows  $\beta$ -cristobalite which was produced in a thin foil by heating for one hour at 1000 °C. The oxide grains, which were contained within the amorphous layer, were identified by their diffraction patterns. This figure demonstrates the major difficulty associated with examining  $\text{SiO}_2$  in an electron microscope, namely the vitrification that occurs rather quickly[14]. As shown in Fig. 3, the  $\beta$ -cristobalite transformed to a disordered  $\alpha$ -cristobalite which then transformed to amorphous silica without changing shape. A similar decomposition occurred in all of the samples regardless of the oxidation conditions. This diffraction pattern of the transformed amorphous silica was used as a standard pattern for silica glass.

Magnesium Silicate-MgSiO<sub>3</sub>. The magnesium silicate phase, enstatite, was found in sections of specimens that were oxidized at 1200 °C and 1400 °C. The enstatite was found to coexist with β-cristobalite forming a well-sintered layer. Figure 5 shows an example of the layer morphology. In this figure the β-cristobalite has vitrified as expected, while the enstatite remained unchanged during long time electron irradiation. The enstatite grains were usually faulted and had a microstructure similar to the natural mineral [15].

Both cristobalite and enstatite can be produced by devitrification of magnesium silicate glass at 1400 °C [16]. At 1400 °C the stable crystalline phase is protoenstatite while clinoenstatite forms on cooling below 1000 °C. Enstatite belongs to the mineral class of pyroxenes which vary in structure according to the impurities in them. The element analysis shows that the magnesium silicate layer contains Fe, Ca, Al and other impurities commonly found in hot-pressed silicon nitride. The presence of these impurities in the oxide scale in quantities sufficient to form variants of the pyroxenes is evidence for diffusion from the matrix to the oxide scale. In sampling specimens from the mechanical test specimens, it was noted that the occurrence of enstatite coincided with the rapid degradation of strength and the rapid dissolution of the ground surface [8,9].

## (2) DIFFUSION REACTION ZONE

The microstructure of the diffusion reaction zone (DRZ) was examined using thin sections of specimens that were oxidized by heating in air 50 hours at 1100°C, 200 hours at 1200°C and 1 and 14 hours at 1400°C. Oxidation in the diffusion reaction zone appeared to initiate at grain boundaries as evidenced

either by porosity or by thickening of a grain boundary phase. Figure 5 shows an elongated pore between two grains in a sample oxidized at 1400 °C. An example of thickening of the oxide phase between grain boundaries is shown in Fig. 6 where the breadth of the phase is indicated by the moiré fringe pattern. At this temperature, the evidence for creep and plastic deformation in the bulk specimens was shown by extensive dislocation interactions in the diffusion reaction zone. There is a significant increase in the occurrence of grain boundary dislocations, sub-boundaries, and dislocation interactions with inclusions as in Figs. 5 and 6b. Rapid growth of oxide at the grain boundaries can produce considerable stress; and, this extended phase can fracture on cooling to produce extensive grain boundary cracking and a new flaw population.

Evidence for nucleation and growth of  $\text{Si}_2\text{N}_2\text{O}$  within the silicon nitride grains is shown in Fig. 7. This foil was made from a specimen that was oxidized for 24 hr. at 1000 °C and had an oxide scale composed of amorphous silica and  $\beta$ -cristobalite. The presence of such plates in the matrix grains could reduce fracture toughness by providing easy intragranular fracture paths along the fault planes.

The early stages of void or particle nucleation within silicon nitride grains is seen in Fig. 8a. The specimen was oxidized for 50 hours at 1100°C. The area shows dislocation loops and stacking faults lying in rhombohedral planes. The small bubbles or precipitates are intersected by dislocations passing through the bulk of the grain. Similar defects are seen in Fig. 8b which shows a specimen that was oxidized during a static load test that lasted

1000 hours at 1200°C. These grains are approximately 20  $\mu\text{m}$  from the oxide : matrix interface.

### (3) INCLUSIONS

The grinding particle inclusions seen in foils made from as-received specimens, are usually polyhedral and range in size from a few nanometers to a few micrometers. The W-based inclusions can be seen as dark masses in thin sections ( $\sim 30\mu\text{m}$ ) examined with a light microscope as in Fig. 9a. The spacial distribution of the individual particles can be seen using the back-scattered electron mode and the transmission mode of imaging in the scanning transmission electron microscope. In the scanning transmission mode as in the normal transmission mode the particles are imaged with the microstructural background of grain boundaries as in Fig. 9b. By using the back-scattered mode the heavy element particles are imaged in Fig. 9c, as dark against the light background and the stereo pictures show three-dimensional distribution of particles. Small particles are found along grain boundaries and within grains. The larger particles are close to or larger than matrix grains. Energy dispersive analysis shows Fe, Cr, Co, Al, and W from the WC and  $\text{WSi}_2$  particles and the metal alloy binder.

Oxidation at the inclusions broken off from the WC grinding media can lead to the formation of oxide filled pits in the matrix and mounds or depressions in the oxide scale. Such pits were shown to be active fracture sites in specimens broken at 1200 °C; and the oxide scale at the pit was found to have a high Fe content [8]. In oxidized specimens these inclusions may be polyhedral or spherical and examples are shown in Fig. 10. The inclusion in

Fig. 10a is surrounded by an amorphous film and this early oxidation reaction is a precursor to an oxide-filled pit. The large spherical particles in Fig. 10b had a high Fe and Cr content but low W content; and, these differences in morphology and composition indicate possible melting or rapid volatilization during the exposure at 1400 °C. The oxidation pits are new flaws which affect the strength in a time dependant manner because they require an incubation time to be produced. Since the distribution of the grinding particle inclusions varies somewhat from billet to billet, the nucleation and growth of the oxidation pits will vary also to change the flaw population.

#### IV. DISCUSSION

The results presented here represent the starting point for further analyses of the relationships between microstructure and high temperature mechanical properties of silicon nitride. Because this ceramic oxidizes, its high temperature behavior as a structural material must be catagorized with its oxidation behavior. By the time cavitation creep and finally creep rupture occur the material has exceeded the limits of usefulness in any structural application. The defects identified in the diffusion reaction zone appear to be related to impurity content and therefore can give some clues to the differences in behavior between billets of the same nominal composition and manufacturing conditions. For example, the defects shown in Fig. 8 were not found in a companion billet which exhibited slightly different strength behavior. Cavities that nucleate and grow near and along grain boundaries create a new flaw population that can cause weakening and failure when the cavities link up to produce grain boundary cracks.

The effect of flaws, such as machining cracks which intersect the surface, on the strength can be changed by oxidation which blunts them or shortens them. When the matrix is consumed by the growing oxide as shown in Fig. 2 then the crack size is reduced and the strength is increased. The time frame for such crack healing is related to the transformation of oxide scale from oxynitride and silica to the silica and silicate. A sharp crack can be blunted when the interfacial matrix grains oxidize. A blunt crack requires a higher stress intensity factor for propagation which leads to a higher strength. Additionally the strain relief resulting from annealing at 1200°C can change the effective stress in ground surfaces and at crack tip. Thus any of these three effects can cause a strengthening. We have shown here that, in the billets studied oxidation can change the strength by reducing the effectiveness of old flaws and by generating new flaws. The specific causes of billet to billet variation in strength and oxidation behavior have not been determined but are believed to be related to impurity content. The oxide scales are similar in composition but have grown at considerably different rates apparently as a result of minor impurity differences. The real effect of annealing in the absence of oxygen will have to be examined in neutral atmosphere tests.

The interaction of the different oxide phases with each other and with the silicon nitride matrix is time and temperature dependent. As long as only silicon oxynitride and crystalline and amorphous silica cover the exposed surfaces, the oxidation rate is slow and the oxide scale is protective. Diffusion of oxygen through the oxide scale is then rate controlling. When sufficient diffusion of Mg and Ca impurities from the matrix has occurred to permit growth of the pyroxene phase then the oxidation reaction can change

rapidly. The diffusion reaction zone illustrated in this paper is more complex than the original matrix structure; and, more examples taken from oxidized and deformed samples must be examined to fully characterize this zone. Recent experiments with sialons (silicon-aluminum-oxynitride) have shown that oxidation at 1400 °C for 1000 hr. can be beneficial to the strength as a result of diffusional changes in the microstructure [16]. Specimens of magnesia-doped hot-pressed silicon nitride which have undergone such long annealing treatments during static fatigue tests show some strengthening but these specimens have not been characterized completely to identify the sources of the strengthening.

## V. CONCLUSIONS

The oxide scale on magnesia-doped hot-pressed  $\text{Si}_3\text{N}_4$  forms in layers composed of amorphous and crystalline  $\text{SiO}_2$ ,  $\text{Si}_2\text{N}_2\text{O}$ , and  $\text{MgSiO}_3$  ( $\text{MgO}\cdot\text{SiO}_2$ ). A diffusion reaction zone in the  $\text{Si}_3\text{N}_4$  matrix is produced during oxidation; and, structural changes such as cavitation in this zone affect strength. Flaw healing and flaw generation occur as a consequence of the growth of oxide phases at and below the  $\text{Si}_3\text{N}_4$  ground surfaces during heating at temperatures > 1000 °C.

## REFERENCES

1. D. R. Clarke and G. Thomas, Grain Boundary Phases in Hot-Pressed MgO Fluxed Silicon Nitride, *J. Amer. Ceram. Soc.* 60, 491-95 (1977).
2. A. H. Heuer, V. Lou, L. Ogbugji, and T. E. Mitchell, Lattice Resolution Studies of Engineering Ceramics: SiC and Si<sub>3</sub>N<sub>4</sub>, *J. Microsc. Spec. Electron* 2, 475 (1977).
3. N. J. Tighe, Microstructure of Oxidized Silicon Nitride, *Proc. EMSA* p. 470-71 (1974) Claitor Publ. Baton Rouge.
4. S. C. Singhal, Thermodynamics and Kinetics of Oxidation of Hot-Pressed Silicon Nitride, *J. Mat. Sci.* 11, 500 (1976).
5. A. G. Evans and S. M. Wiederhorn, Proof Testing of Ceramic Materials, An Analytical Basis for Failure Prediction, *Int. J. Fracture*, 10, 379-92 (1974).
6. S. M. Widerhorn and N. J. Tighe, Effects of Oxidation on the Reliability of Si<sub>3</sub>N<sub>4</sub>, in "Fracture Mechanics of Ceramics", Vol. 5 & 6, R. C. Bradt, A. G. Evans, D. P. H. Hasselman and F. F. Lange, eds. Plenum Publ. 1982.
7. F. F. Lange, "Evidence for Cavitation Crack Growth in Si<sub>3</sub>N<sub>4</sub>", *J. Am. Ceram. Soc.* 62 [3-4], 222-23 (1979).
8. S. M. Wiederhorn and N. J. Tighe, Proof-Testing of Hot-Pressed Silicon Nitride, *J. Mat. Sci.* 13, 1781 (1978).
9. S. M. Wiederhorn and N. J. Tighe, Effect of Flaw Generation on Proof Testing, MCIC Report, March 1978 p. 689.
10. S. M. Wiederhorn, A Probabilistic Framework for Structural Design in "Fracture Mechanics of Ceramics, Vol. 5 & 6, R. C. Bradt, A. G. Evans, D. P. H. Hasselman and F. F. Lange, eds. Plenum Publishing Corp., 1982.

11. I. Idrestedt and C. Brosset, Structure of  $\text{Si}_2\text{N}_2\text{O}$ , Acta Chem. Scand. 18, 1879 (1964).
12. C. A. Anderson, K. Keil, and B. Mason, Silicon Oxynitride: A Meteoritic Mineral, Sci. 146, 256 (1964).
13. D. Taylor, Reflected Light Microscopy of Silicon Nitride and Oxynitride, T. Brit. Ceram. Soc. 72, 319-21 (1973).
14. N. J. Tighe and J. M. Christie, Deformation Structures in Quartz Rocks, Proc. EMSA p. 60-61 (1969) Claitor Publ. Baton Rouge.
15. P. E. Champness and G. W. Lorimer, Precipitation in an Orthopyroxene, J. Mat. Sci. 8, 467 (1973).
16. L. Atlas, The Polymorphism of  $\text{MgSiO}_3$  and Solid-State Equilibria in the System  $\text{MgSiO}_3$ - $\text{CaMgSi}_2\text{O}_6$ , J. Geol. 60, 125 (1952).
17. M. H. Lewis and P. Barnard, Oxidation Mechanisms in Si-Al-O-N Ceramics, J. Mat. Sci. 15, 443 (1980).

#### ACKNOWLEDGEMENTS

This work was supported in part by the Office of Coal Utilization, Div. of Heat Engines and Heat Recovery, Department of Energy Contract EA77-A01-6010 Task A086. We thank C. M. McDaniel for the careful X-ray diffraction analyses.

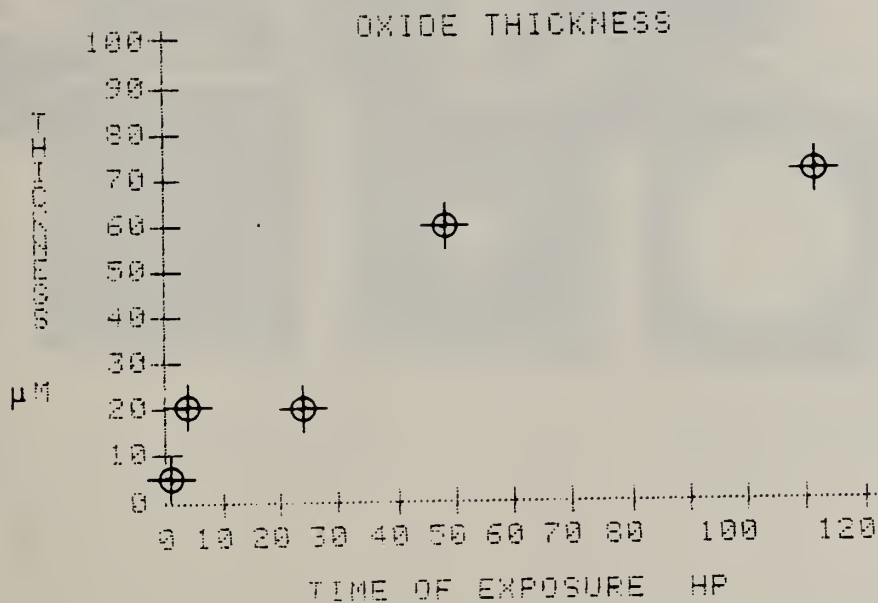
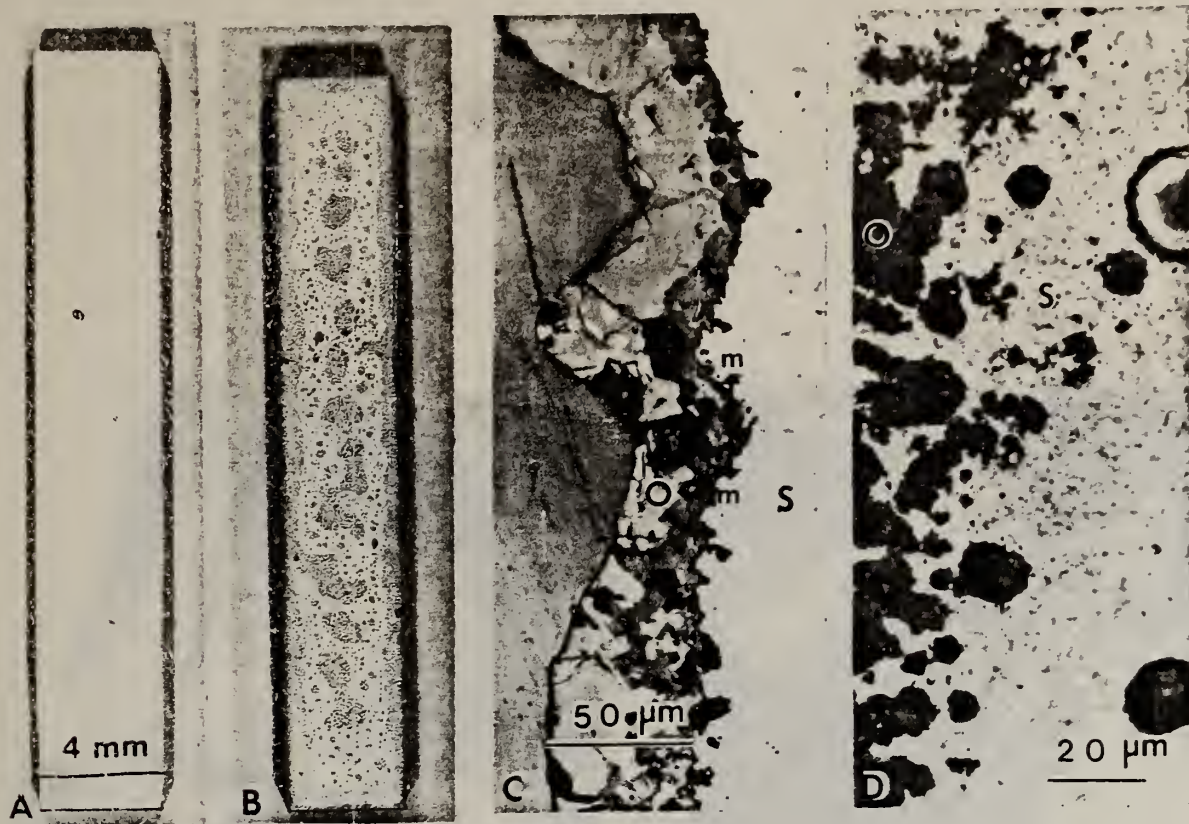


Fig. 1. Hot-pressed silicon nitride samples which were oxidized at 1400°C (A) specimen heated continuously for 100 hr., (B) specimen heated and cooled to room temperature several times during 96 hr., (C) polished section of cyclically heated specimen note thickness variations in oxide scale -O- and in  $\text{Si}_3\text{N}_4$  -S-. (D) nodules of  $\text{Si}_2\text{N}_2\text{O}$  below the primary oxide-matrix interface spec. (E) plot of scale thickness vs time for NC 130 specimens.

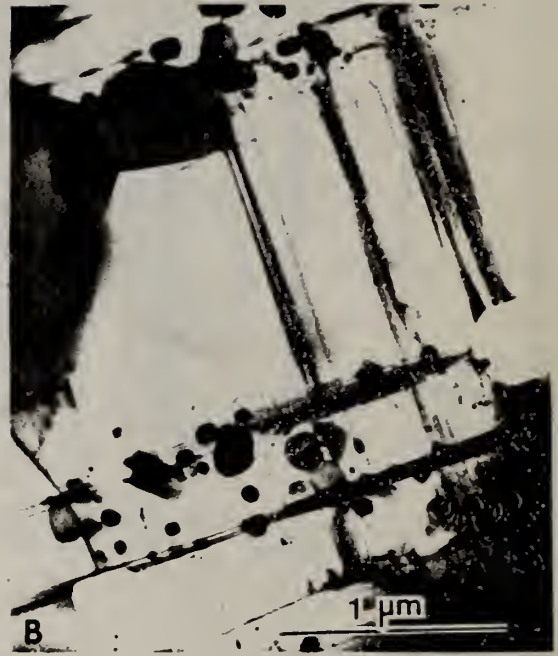


Fig. 2. Electron micrographs of sections from specimen heated 264 hr. at 1000°C showing (A) 2  $\text{Si}_2\text{N}_2\text{O}$  grains within the  $\text{Si}_3\text{N}_4$ , (B) enlargement of oxynitride grain showing faults, pores and precipitates.

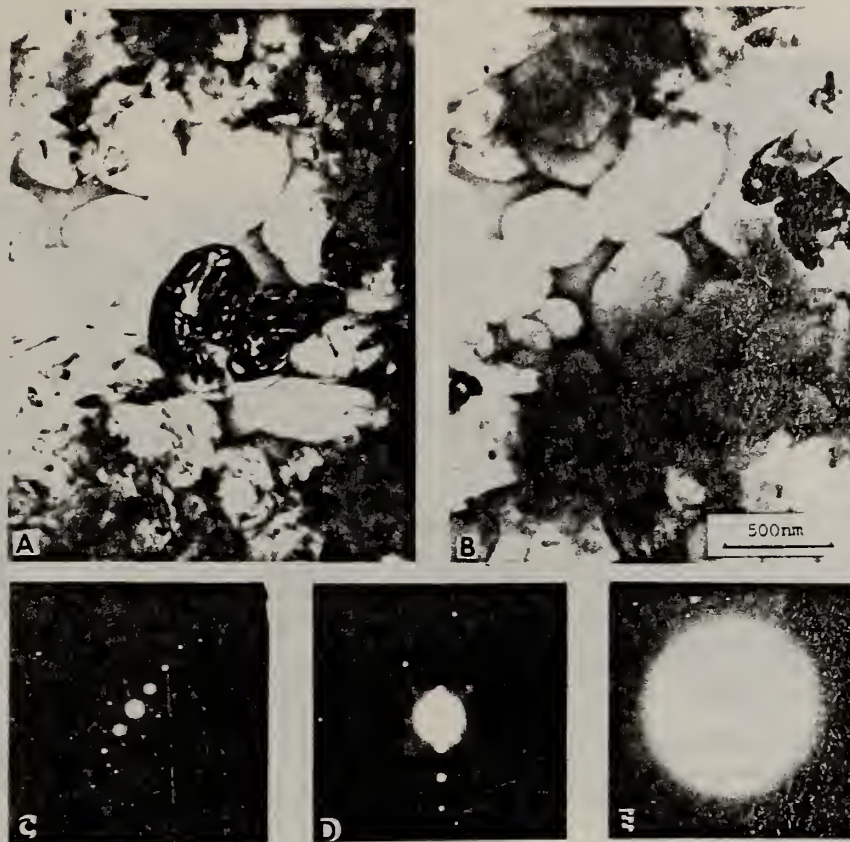


Fig. 3. Thinned Si<sub>3</sub>N<sub>4</sub> foil after heating 1 hr. at 1000°C, thin area oxidized completely to cristobalite and glass; (A) SiO<sub>2</sub> grains, (B) vitrified SiO<sub>2</sub>, (C,D,E) diffraction patterns of the transformation βSiO<sub>2</sub> → αSiO<sub>2</sub> → amorphous SiO<sub>2</sub>.

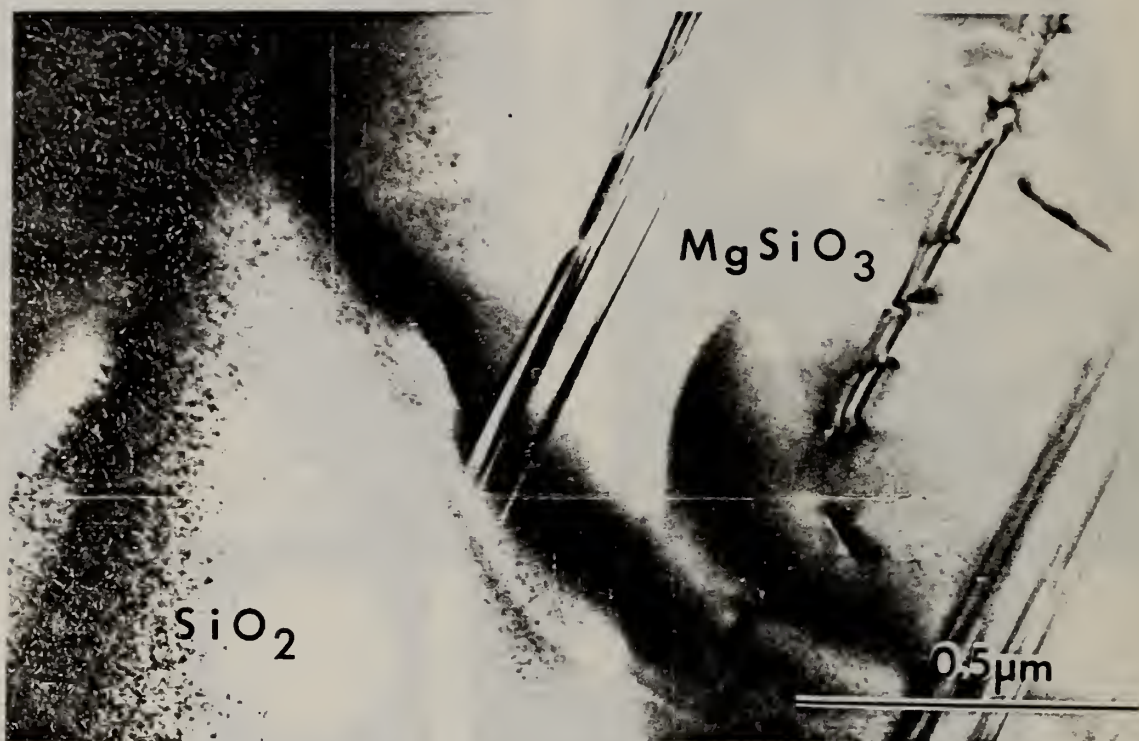


Fig. 4. Oxide scale from bulk specimen heated at  $1400^\circ\text{C}$  showing grains of  $\text{SiO}_2$  and  $\text{MgSiO}_3$ , note the  $\text{SiO}_2$  grain has vitrified.



Fig. 5. Silicon nitride grains in specimen heated 24 hr. at 1400°C, large pore is seen along grain boundary (arrowed).

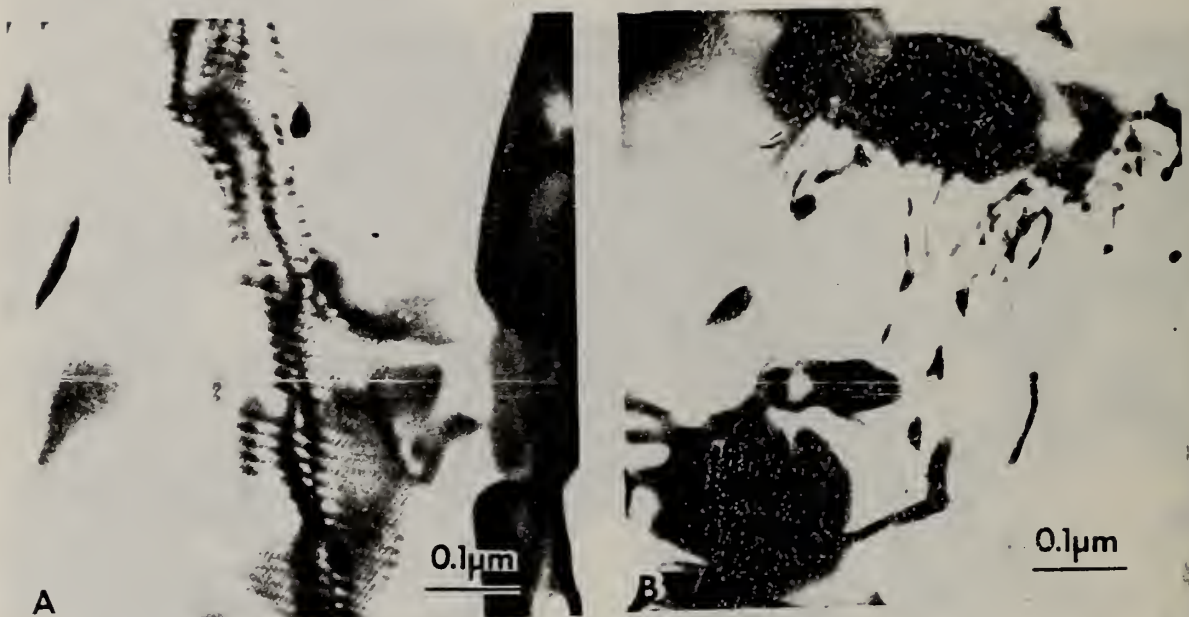


Fig. 6. Section from bar heated cyclically for 96 hr. at 1400°C showing:  
(A) Silicon nitride grains in the diffusion reaction zone, moiré fringes along the boundary show position of the growing oxide film.  
(B) Dislocation interactions with inclusions near area in (A).

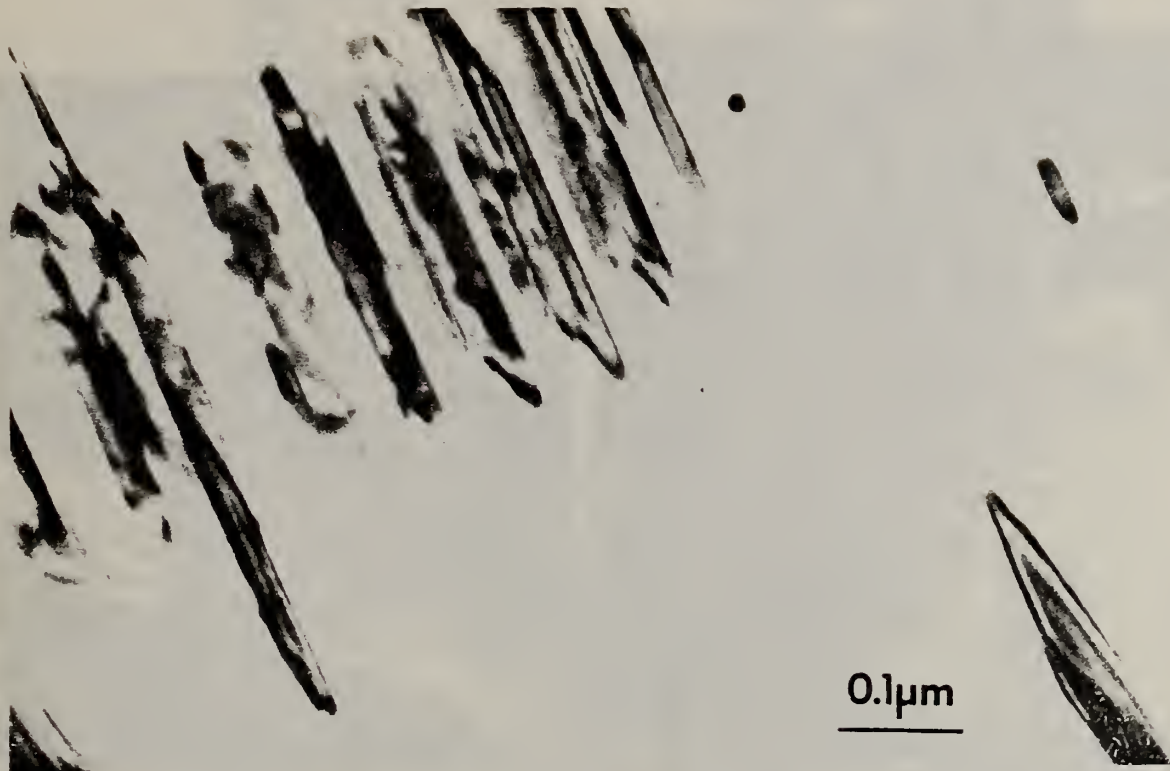


Fig. 7. Grain of Si<sub>3</sub>N<sub>4</sub> containing plates of Si<sub>2</sub>N<sub>2</sub>O in the diffusion reaction zone of a specimen oxidized 24 hr. at 1000°C.

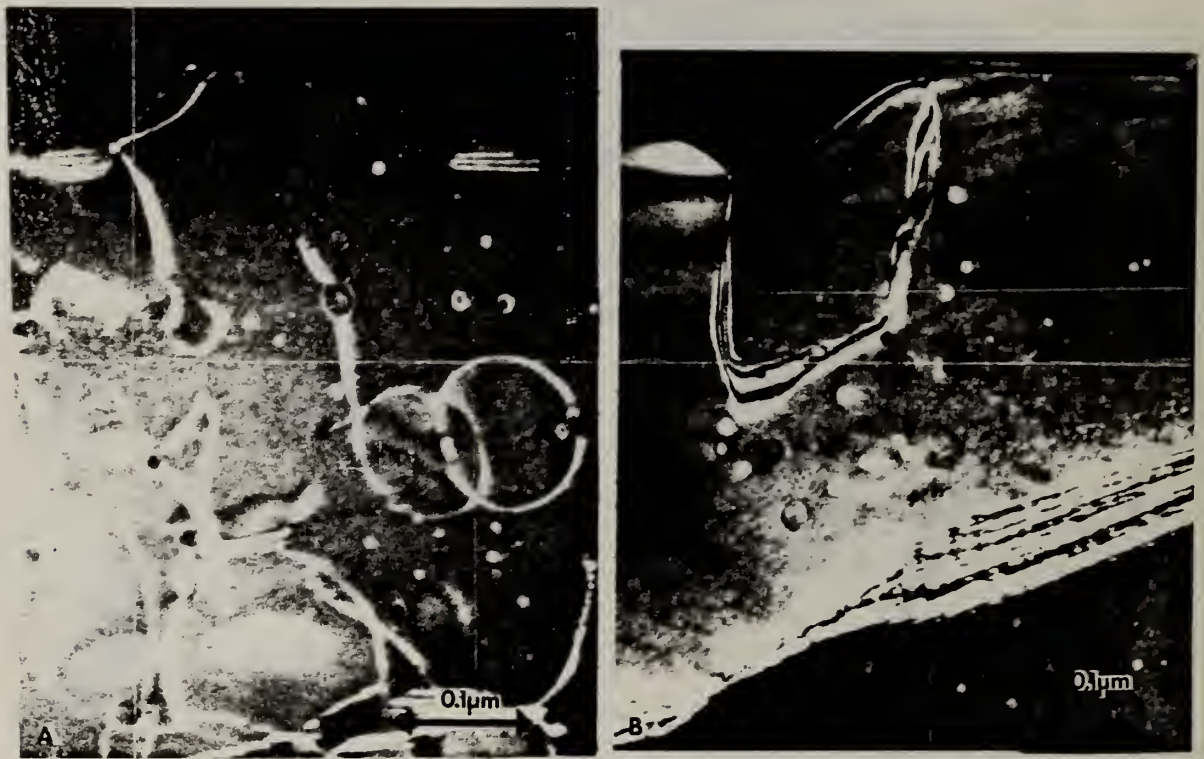


Fig. 8. Oxidation induced cavity and particle nucleation in the diffusion reaction zone of NC132. (A) Oxidized 50 hours at 1100°C dislocation loops lying in rhombohedral plans and are pinned at cavities. (B) Oxidized 1000 hours at 120°C during static load test. The cavities are distributed through the grain thickness.

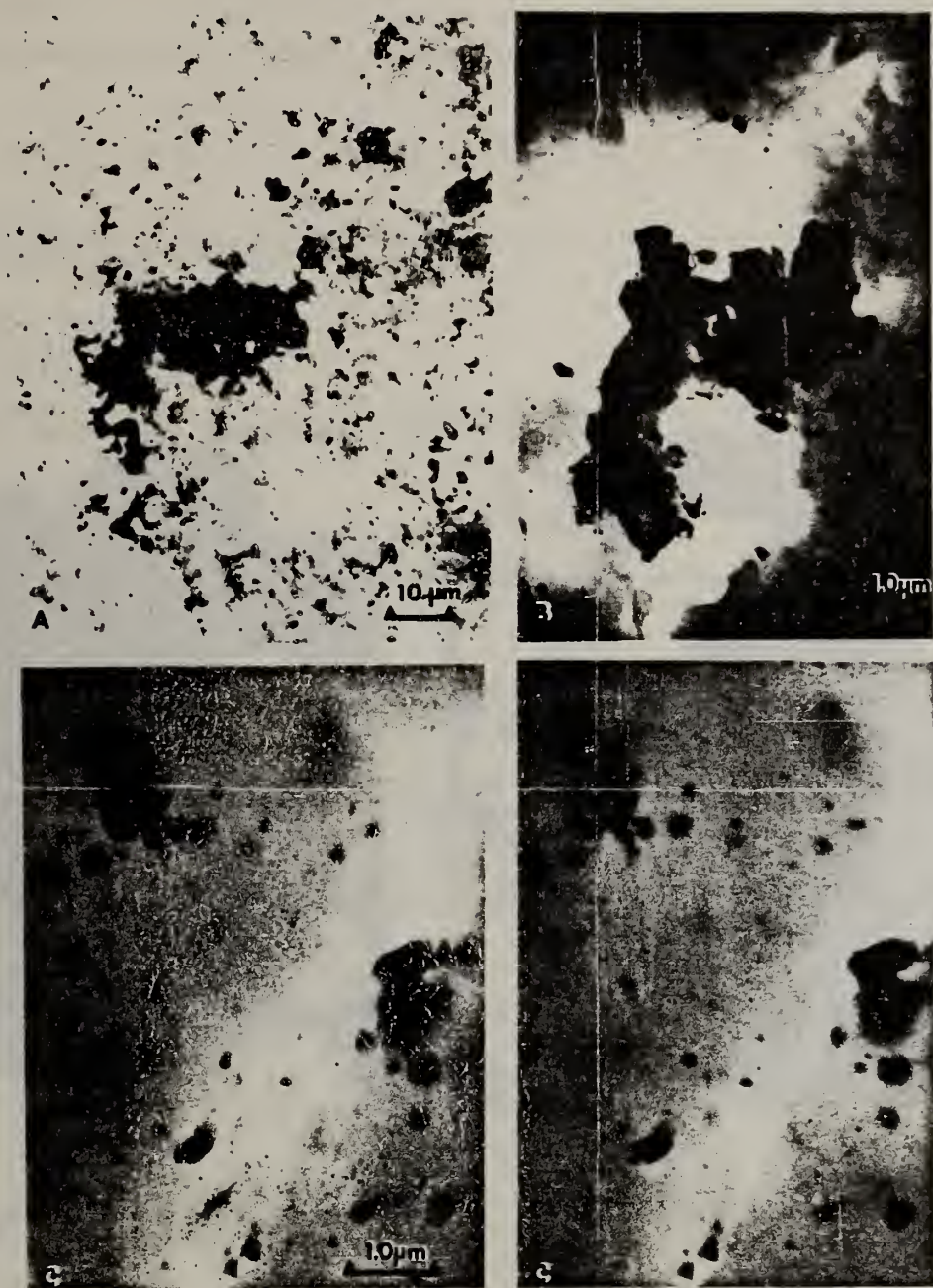


Fig. 9. Spatial distribution of inclusions in silicon nitride (a) transmitted light showing dark inclusion masses, (b) scanning transmission images showing inclusions and silicon nitride grains, (c) stereo-pair of back-scattered electron images showing 3-D view of inclusions.

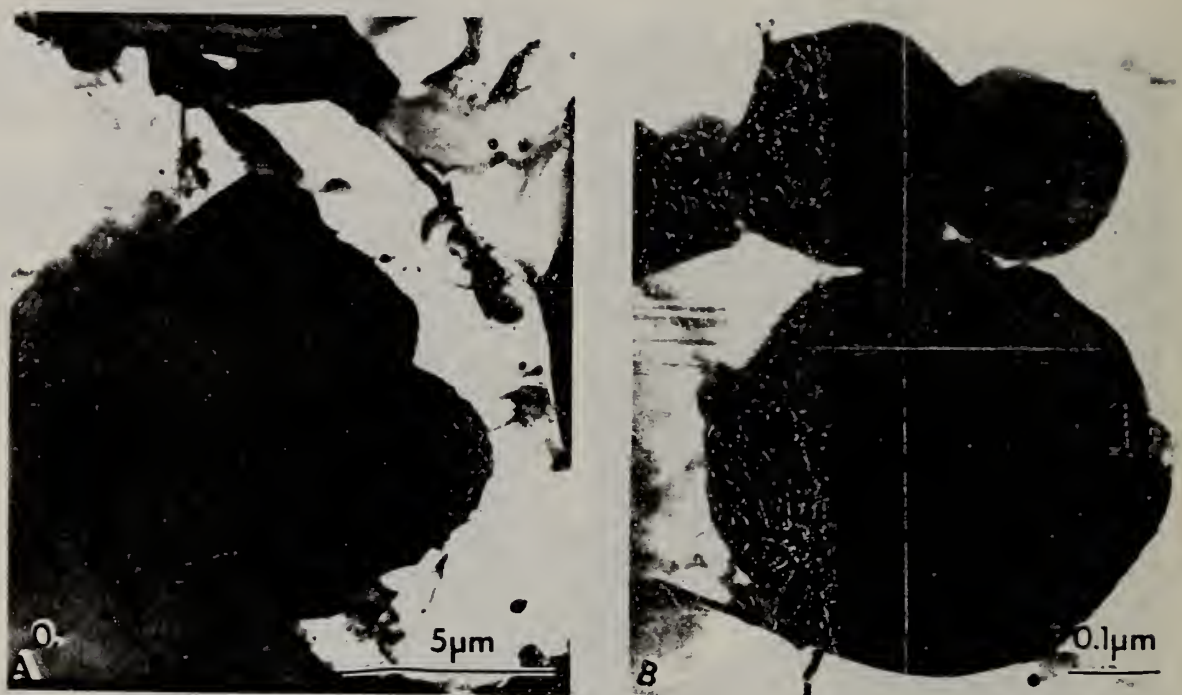


Fig. 10. Inclusions in  $\text{Si}_3\text{N}_4$  specimen heated at  $1400^\circ\text{C}$  (A) in 1 hr. inclusion is surrounded by porous and amorphous phase, indicating that oxidation has started. (B) After 96 hr. of cyclic heating, inclusions are spherical and show no W.

U.S. DEPT. OF COMM. BIBLIOGRAPHIC DATA SHEET	1. PUBLICATION OR REPORT NO.  NBSIR 82-2574	2. Gov't. Accession No.	3. Recipient's Accession No.
4. TITLE AND SUBTITLE  Analysis of Oxide and Oxide + Matrix Interfaces in Silicon Nitride		5. Publication Date	
7. AUTHGR(S)  Nancy J. Tighe		6. Performing Organization Code	
9. PERFORMING ORGANIZATION NAME AND ADDRESS  NATIONAL BUREAU OF STANDARDS DEPARTMENT OF COMMERCE WASHINGTON, DC 20234		8. Performing Organ. Report No.	
12. SPONSORING ORGANIZATION NAME AND COMPLETE ADDRESS (Street, City, State, ZIP)		10. Project/Task/Work Unit No.	
15. SUPPLEMENTARY NOTES  <input type="checkbox"/> Document describes a computer program; SF-185, FIPS Software Summary, is attached.		11. Contract/Grant No.	
16. ABSTRACT (A 200-word or less factual summary of most significant information. If document includes a significant bibliography or literature survey, mention it here.)  In order to understand the strength and microstructural changes that are produced during oxidation, it is necessary to examine the oxide scale, the oxide:silicon nitride interface and the silicon nitride below the oxide:matrix interface. In the present study, these three interfacial layers were removed and analyzed using transmission electron microscopy, light microscopy, x-ray energy analysis and x-ray diffraction. Oxide scales were produced on hot-pressed silicon nitride samples by heating in air at 1000 °C, 1200 °C, and 1400 °C for 1/2 to 1000 hr. The phases in the oxide scale were found to occur in layers that were ordered according to the phase diagrams for the oxide mixtures. Crystalline and amorphous phases were present in all specimens examined. The oxynitride and amorphous phases are present in as-pressed billets at triple junctions and along grain boundaries. The elements in the amorphous phases were identified using energy dispersive x-ray analysis. In this paper, the phases found in the oxide scales are characterized and the relationships between the oxide scale, the oxide:matrix interface and the mechanical properties are discussed.		13. Type of Report & Period Covered Symposium and NBSIR	
17. KEY WORDS (six to twelve entries; alphabetical order; capitalize only the first letter of the first key word unless a proper name; separated by semicolons) Silicon nitride; electron microscopy; oxidation; microstructure; analysis; TEM; STEM; enstalite; $\beta$ crystalalite; silica; silicates.		14. Sponsoring Agency Code	
18. AVAILABILITY  <input checked="" type="checkbox"/> Unlimited  <input type="checkbox"/> For Official Distribution. Do Not Release to NTIS  <input type="checkbox"/> Order From Sup. of Doc., U.S. Government Printing Office, Washington, DC 20402, SD Stock No. SN003-003-  <input type="checkbox"/> Order From National Technical Information Service (NTIS), Springfield, VA. 22161	19. SECURITY CLASS (THIS REPORT)  UNCLASSIFIED	21. NO. OF PRINTED PAGES	
	20. SECURITY CLASS (THIS PAGE)  UNCLASSIFIED	22. Price	





